NUMERICAL SIMULATION OF FLOWS AROUND A NACA 0012 AIRFOIL IN TRANSIENT PITCHING MOTION USING IMMERSED BOUNDARY METHOD WITH VIRTUAL PHYSICAL MODEL

José Eduardo Santos Oliveira
Laboratory of Heat and Mass Transfer and Fluid Dynamic – University Federal of Uberlândia
Mechanical Engineer College – Bloco 1M – Av. João Naves de Ávila, 2.121. CEP 38400-902
e-mail: jeolivei@mecanica.ufu.br

Ana Lúcia Fernandes de Lima e Silva
e-mail: alfsilva@mecanica.ufu.br

Aristeu da Silveira Neto
e-mail: aristeus@mecanica.ufu.br

Abstract. *In the present work the numerical simulation of turbulent flow over airfoils in transient pitching moving is presented. The flow is simulated through the numeric solution of the Navier-Stokes equations using the Immersed Boundary Method with Virtual Physical Model. This methodology allows the modelling of complex geometries immersed in the flow. With the use of two independent meshes there is no restriction as the movement or deformation of the body. In this way, the simulation of the flow on moving boundaries does not present any additional difficulty, as it happens in the classic methods where the meshes must be reconstructed. It is presented the two-dimensional simulation of flow past a NACA 0012 airfoil profile in oscillating pitching for two different moving speeds in order to evaluate the transient effect on the flow. Preliminary numerical results presented a good physical coherence.*

Keywords*: Immersed Boundary Method, Virtual Physical Model, Airfoils, Moving Boundaries*

1. Introduction

Dynamic stall is a term used to describe a process where the normal force sudden drop, while the airfoil increases the attack angle through a pitch motion. The stall phenomenon for thin airfoils is often associated with the formation of a leading-edge vortex and is generally preceded by laminar boundary-layer separation near the airfoil nose. The vortex travel along the airfoil surface as it grows, and finally separates from the airfoil at its trailing edge. Dynamic stall is an unsteady phenomenon and differently of static stall the flow separation occurs at high angle-of-attack. A complete understanding of the dynamics of leading edge separation on a pitching airfoil is essential to design of compressor blades, wings of modern fighters, helicopters, etc. The dynamic stall phenomena was first study by the helicopter industries, where large torsional oscillations of the blades was observed and attributed to the periodic stalling and unstalling of each blade on the retreating side of the rotor disk (Akbari and Price, 2003).

To model the moving airfoil immersed in the flow it is represented by immersed boundary method (IB). The IB method was proposed by Peskin (1977) to simulate blood flow in heart valves, a high complex problem that involves moving boundaries and complex geometries. The main idea of the Peskin method is to use two meshes. The Eulerian mesh is used to solve the fluid flow equations while an independent Lagrangian mesh represents the immersed body. The interaction between the two meshes is made through a force source term added to the Navier-Stokes equations. This procedure allows to model complex geometries immersed in a fluid flow, avoiding the use of complex meshes to fit the grid to the immersed body. As a geometric dependence does not exist between these two meshes, the immersed boundary method can easily handle moving boundary problems without regenerating grids in time. The main issue in the methods, based on the concept of immersed boundary, is how to compute the force term. In the present work, a new model named Virtual Physical Model (VPM) proposed by Lima e Silva *et al.* (2003), is used. It is based on the calculation of the force field over a sequence of Lagrangian points, which represent the interface, using the Navier-Stokes equations.

In the present work, preliminary numerical results of an oscillating airfoil at Reynolds number 10^4 is presented. The airfoil was submitted to a harmonic pitching motion about the mid-chord axis at two reduced frequencies: 0.5 and 0.25. The mean incidence and the oscillating amplitude were 5^o and 10^o. The turbulence modeling methodology used was the Large Eddy Simulation (LES) with the Smagorinsky algebraic sub-grid scale model to calculate the turbulent viscosity. A qualitative comparison is made between the two simulated cases evidencing the effect of reduced frequency on the aerodynamic force coefficients and fluid flow behavior.

2. Mathematical Formulation

The main idea in the IBM/VPM methodology is to solve the flow over immersed bodies using two independent meshes: a fixed Eulerian mesh for the fluid domain and a Lagrangian mesh to represent the solid-fluid interface. There are no difficulties to represent complex immersed bodies, related to the mesh building.

2.1. Mathematical Model for Fluid Domain

A rectangular domain was used for the present simulations and it was discretized with an Eulerian grid. The Navier-Stokes equations for a viscous incompressible fluid can be written as:

$$\rho\left[\frac{\partial u_i}{\partial t}+\frac{\partial\left(u_i u_j\right)}{\partial x_j}\right]=-\frac{\partial p}{\partial x_j}+\frac{\partial}{\partial}\left[\left(\nu+\nu_t\right)\left(\frac{\partial u_i}{\partial x_j}+\frac{\partial u_j}{\partial x_i}\right)\right]+f_i, \tag{1}$$

$$\frac{\partial u_i}{\partial x_i}=0. \tag{2}$$

It must be stressed that Eq. (1) is already the filtered equation. Also, the Boussinesq hypothesis was used to model the subgrid Reynolds stress tensor. These equations are solved on the Eulerian mesh and the coupling between the two meshes is made by the force source term f_i that is different from zero only over the immersed boundary. Equation (3) models the interaction between the immersed boundary and the fluid, by the distribution of the Lagrangian force on the fluid:

$$\vec{f}\left(\vec{x}\right)=\int_{\Gamma}\vec{F}\left(\vec{x}_k,\ t\right)\delta\left(\vec{x}-\vec{x}_k\right)d\vec{x}_k, \tag{3}$$

where $\vec{F}$ is the Lagrangian force density placed on $\vec{x}_k$ points over the interface Γ and $\delta(\vec{x}-\vec{x}_k)$ is the Dirac delta function.

In order to discretize Eq. (3), the Dirac delta function is replaced by a distribution function D_{ij}. This function acts like a Gaussian weighting function with a unitary integral over the interval $[-\infty,+\infty]$. Therefore, Eq. (3) is replaced by:

$$\vec{f}\left(\vec{x}\right)=\sum D_{ij}\left(\vec{x}-\vec{x}_k\right)\vec{F}\left(\vec{x}_k,\ t\right)\Delta s^2, \tag{4}$$

where Δs is the distance between two Lagrangian points.

2.2. Solid-Fluid Interface Model

The VPM performs the dynamic evaluation of the force exerted by the fluid flow over the immersed body. The force density $\vec{F}(\vec{x}_k,t)$ is calculated over the Lagrangian points using the momentum equations. The Lagrangian force can be expressed by:

$$\vec{F}_i\left(\vec{x}_k,t\right)=\frac{\partial u_i}{\partial t}+\frac{\partial p}{\partial x_i}+\frac{\partial\left(u_i u_j\right)}{\partial x_j}-\frac{\partial}{\partial x_j}\left[\nu\left(\frac{\partial u_i}{\partial x_j}+\frac{\partial u_j}{\partial x_i}\right)\right] \tag{5}$$

The different terms on the right hand side of Eq. (5) are referred as: acceleration force, pressure force, inertial force and viscous force. The four components of force density $\vec{F}(\vec{x}_k,t)$ are calculated on a control volume centered at a Lagrangian point, $\vec{x}_k$.

To evaluate the different terms described by Eq. (5) the pressure $p(\vec{x},t)$ and the velocity $\vec{V}(\vec{x},t)$ fields must be known previously. These fields are calculated on the Eulerian grid while the force terms must be calculated over the interface. One of the possible ways to do that is to interpolate $\vec{V}(\vec{x},t)$ and $p(\vec{x},t)$ over appropriate auxiliary Lagrangian points near the interface, as illustrated by Lima e Silva *et al.* (2003).

For the pressure field, only grid points external to the interface and at a distance less than or equal to $2\Delta x$ are used in the interpolation process. For the velocity fields the external and internal points are taken, because the internal velocity field helps to model virtually the no-slip boundary condition. The pressure and velocity derivatives that appear in Eq.(5), are calculated using a second order Lagrange polynomial approximation.

3. Turbulence Modelling

The Navier-Stokes equations are able to simulate, with fairly good agreement, a wild range of engineering problems including high complex unsteady turbulent flows. However, it is necessary to solve all degrees of freedom of the flow, which is proportional to $Re^{9/4}$. This technique is called DNS (*Direct Numerical Simulation*) and it is obviously restricted to low Reynolds number due to the high mesh resolution required, considering the nowadays computers.

An alternative way to handle this problem is the use of Reynolds decomposition or general filtering process of Germano (1986). The governing equations are suitably filtered and this procedure gives rise to the closure problem. This closure problem is nowadays solved using turbulence models. Different methodologies have been employed in the turbulence modeling, i. e., LES (*Large Eddy Simulation*). In the LES methodology the largest turbulent structures are solved from the filtered equations and the interaction between the smallest structures and the largest structures is modeled. These small structures are more homogeneous and isotropic (Silveira-Neto, 2003). The scale of the small structure is evaluated from the mesh used to solve the filtered equations, i.e., the filter width becomes a function of the grid. The turbulent structures that are smaller than the grid resolution are modeled by the so-called subgrid-scale models.

In the present work the Smagorinsky subgrid-scale model was employed. The formulation of this model is discussed in the following section.

3.1. Smagorinsky Sub-grid Scale Model

In the present work LES methodology proposed by Smagorinsky (1963) is applied. The sub-grid scale model, which is based on the balance of production of sub-grid scale turbulent kinetic energy and dissipation of isotropic turbulence energy, is used.

The turbulent viscosity is computed as function of strain rate (S_{ij}) and the length scale (ℓ):

$$\nu_t = (C_s \ell)^2 \sqrt{2\bar{S}_{ij}\bar{S}_{ij}}, \tag{6}$$

where $C_S = 0.18$ is the Smagorinsky constant and $\ell = \sqrt{\Delta x \Delta y}$ is the characteristic sub-grid length.

4. Numerical Method

The governing equations, Eq. (1) and (2), were discretized using the central second-order finite difference method in space and a Runge-Kutta second-order scheme in the time. The pressure-velocity coupling was performed using a pressure correction method, as proposed by Chorin (1968). The linear system for the pressure correction was solved using the iterative solver MSI procedure (*Modified Strongly Implicit*) of Schneider and Zedan (1981). The interfacial force field calculation and the momentum equations solution are performed in an explicit way.

All the simulations were carried out on a non-uniform grid. The calculation domain has a length of 10*C* and a width of 8*C*, where *C* is the airfoil chord. A non-uniform grid of 278x198 points with three distinct regions in each direction was used, as can be observed in Fig. (1). On the *x* direction the first section has 50 points and is extended until 2.7*C*. The last section has 5.8*C* of length with 102 points. In the *y* direction the two non-uniform regions are identical with a length of 3.82*C* and *84* points. The airfoil is placed inside a rectangular box with a uniform mesh. The box has dimensions of 1.5*C* x 0.36*C*.

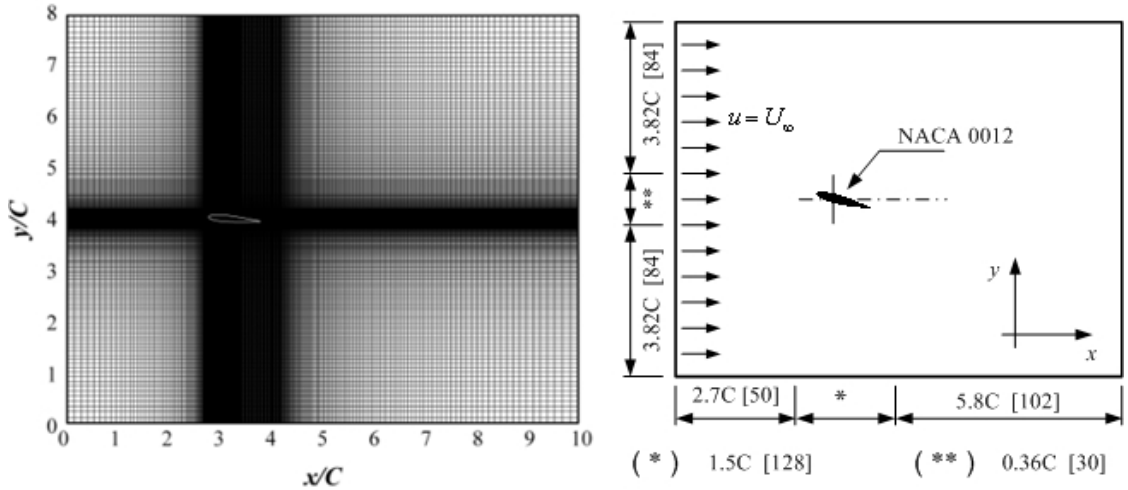

Figure 1. View of the calculation domain.

The airfoil is placed at $3.3C$ from the left boundary and centered vertically at $4C$ and the pitching axe is located at $0.5C$. A constant velocity profile U_∞ was imposed at the domain inlet, in such a way that the fluid goes from the left to the right boundary. Neumann condition was imposed for the velocity at all other faces. For the pressure correction, null derivative was employed at the domain entrance and it was set as zero in the other faces.

It must be stressed that even with the pitching movement, the Eulerian mesh remains unchanged and only the Lagrangian mesh is transported dynamically, following the different angle-of-attack at each time. The angle-of-attack, as a function of time, is given by:

$$\alpha(t) = \bar{\alpha} - \Delta\alpha \cdot cos(\Omega \cdot t), \tag{7}$$

where α is the angle of attack at the time t, $\bar{\alpha}$ is the mean angle-of-attack, $\Delta\alpha$ is the amplitude of the pitching oscillation and $\Omega = 2\pi f$ is the angular velocity, where f is the frequency of oscillation. Usually f is written in terms of the reduced frequency, defined as:

$$\kappa = \frac{\pi f\, C}{U_\infty}. \tag{8}$$

5. Results and Discussions

In this section the preliminary results are presented for the two-dimensional unsteady flow past a pitching NACA 0012 airfoil. The immersed airfoil profile was represented by IB/VPM methodology. The Smagorinsky turbulence model (to perform LES) was employed to simulate two cases at $Re = 10^4$, using the reduced frequencies of $\kappa = 0.5$ and $\kappa = 0.25$. In this work, only one static case was simulated for $\alpha = 5^o$. This case was used to initialize all the pitching simulations. The pitching movement starts from $\alpha = 5^o$ and than the angle is increased in accordance with Eq. (7). The simulation results are present in order to evaluate the effect of the reduced frequency (κ) in the stall phenomena. Results reported by Akbari and Price (2003) predicted the static stall angle at $\alpha \approx 15^o$ for a Reynolds number of 10^4.

Figure (2) shows the dynamic drag (C_D) and normal force (C_N) coefficients for the first test case. This numerical simulation has a mean angle of $\bar{\alpha} = 15^o$, an amplitude of $\Delta\alpha = 10^o$ and a reduced frequency of $\kappa = 0.5$. The simulations were carried out for 4 seconds which is sufficient to the airfoil performs six cycles of oscillations. The lines of Fig. (2) were colored with the time scale to identify each cycle of movement, the coefficients are compared with the numerical simulations of a steady airfoil performed by Akbari and Price (2003). The normal force coefficient predicted for steady angle of 5º was 0.13 against 0.15 from reference; however the drag coefficient is over predicted.

As can be visualized in the Fig. (2), there is a hysteresis loop in the aerodynamic force coefficients. During the downstroke the normal force coefficient is smaller than during the upstroke. This is due to the difference between the flow over the airfoil during these two airfoil movements, which affects significantly the vortex shedding dynamics and mainly the boundary layer detachment/reattachment. During the decrease of the angle of attack, the flow is completely separated and the normal coefficient is reduced. Near $\alpha = 6.5^o$ the normal force increases which is coincident with the flow reattachment on the upper surface. The difference between two consecutive cycles of the hysteresis loop is due to the unsteady nature of the flow.

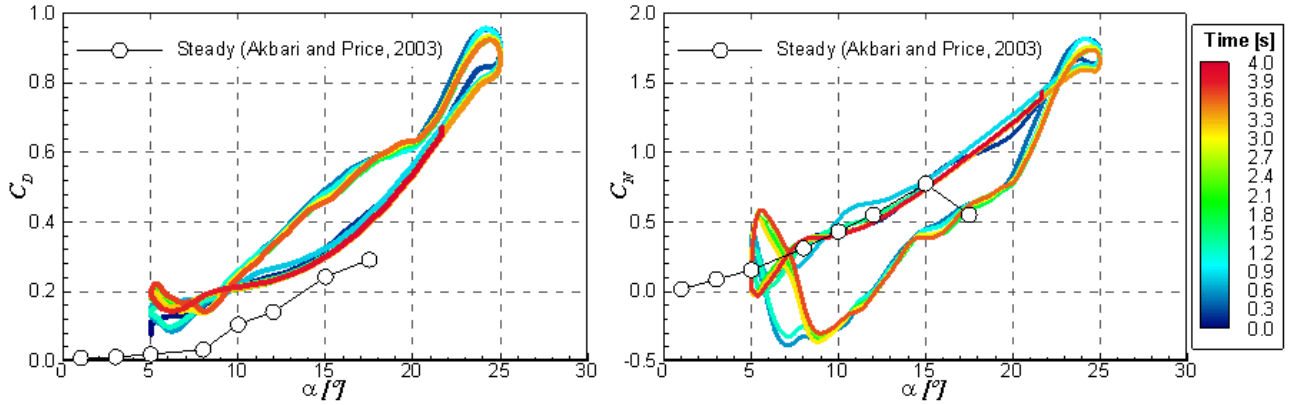

Figure 2. The (a) drag and (b) normal force coefficients versus angle of attack over six oscillation cycles (4 *s*) for the airfoil at $\bar{\alpha} = 15^o$, $\Delta\alpha = 10^o$ and $\kappa = 0.5$

The time evolution of vorticity field ($-150 \le \omega_z \le 150$) for the first cycle of oscillation of the airfoil is presented in Fig. (3). The behavior of aerodynamic forces over the airfoil, showed in Fig. (2), can be associated with the dynamic of vortex shedding presented in Fig. (3). During the upstroke movement a constant increase of the normal force is observed with the increase of the angle-of-attack, and no stall behavior was observed. It can be explained observing the flow over the airfoil, where no apparent indication of flow separation is detected up to $\alpha = 22.4^o$ (Fig. 10g). It is important to note that the static stall occurs at $\alpha = 15^o$. The effect of pitching motion at this reduced frequency inhibits the stall phenomena for this range of angle of attack.

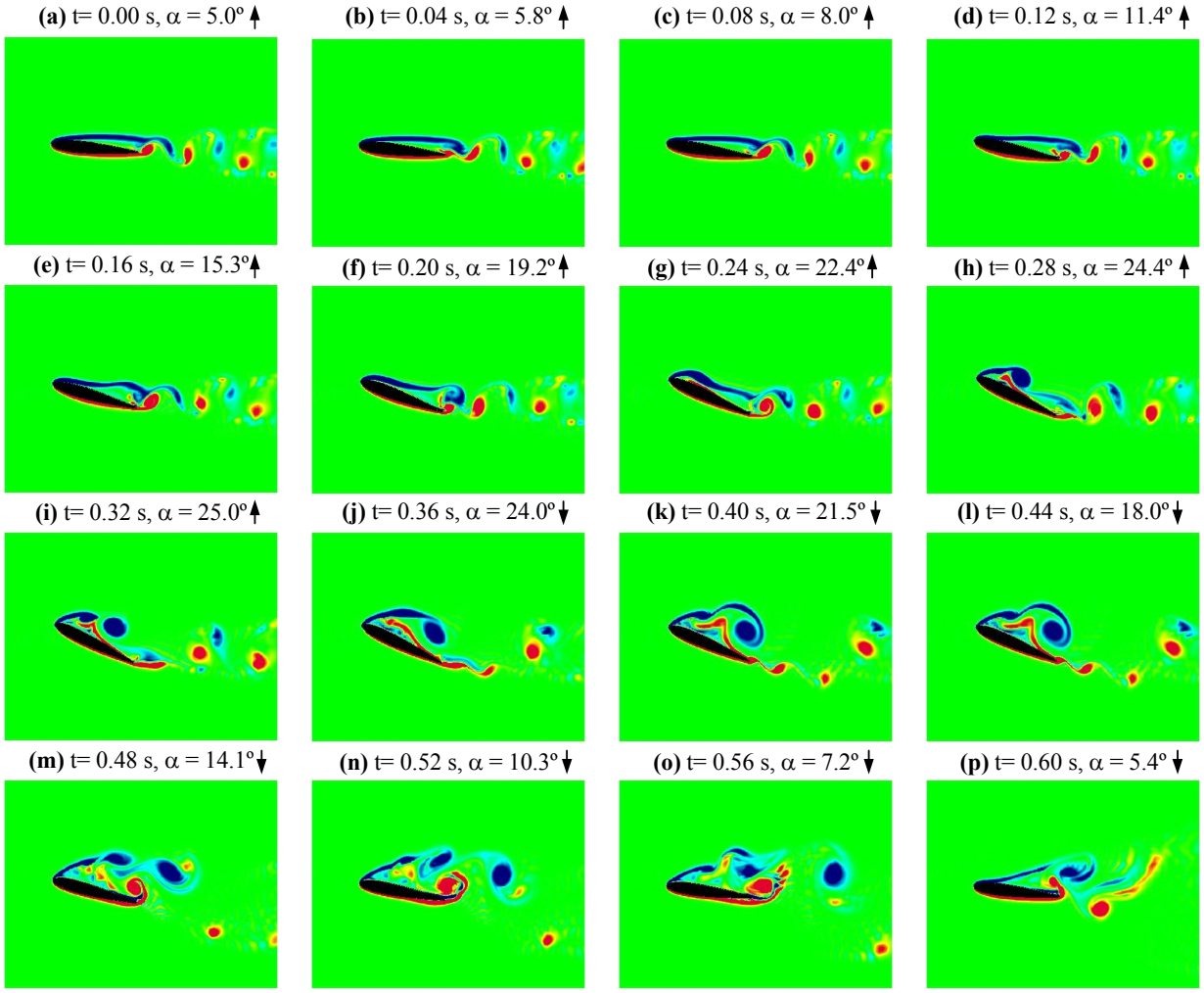

Figure 3. Vorticity field visualization for the NACA 0012 airfoil during the pitching movement at several angles of attack at $\bar{\alpha} = 15^o$, $\Delta\alpha = 10^o$ and $\kappa = 0.5$

At $\alpha = 24.4^o$ (Fig. 3h) a leading-edge separation bubble starts forming over the airfoil. Around this time the airfoil starts the downstroke movement, which forces the vortex shedding at the leading-edge, promoting the detachment of the boundary layer and consequently the drop of the normal force, as shown in Fig. (2). The hysteresis effect in the aerodynamic forces during the downstroke is observed. At $\alpha = 14.1^o$ (Fig. 3m) the growth of a great trailing-edge vortex starts. This vortex is shedded and inhibits the reattachment of the flow. The structures are transported downstream by the flow and around $\alpha = 6.5^o$ occurs the reattachment of the flow and the normal force suddenly increases (Fig. 2b). When α reaches 5.4^o (Fig. 3p), during the downstroke, the flow is already attached at the leading-edge and the time cycle is completed.

Figure (4) shows the drag and normal force coefficients versus the angle-of-attack for the reduced frequency of $\kappa = 0.25$. The simulation was accomplished for 4*s* and the airfoil performed three cycles of oscillation. For this case the normal coefficient also increases during the upstroke movement up to $\alpha = 20^o$. In this angle-of-attack the normal coefficient suddenly drops characterizing the stall point. Note that in the previous case, $\kappa = 0.5$, the stall phenomena was not observed. We can conclude that increasing the reduced frequency the stall angle is delayed to a high value of angle of attack.

It is well know that LES turbulence models are better to describe flow structures and consequently the transient effects of vortices shedding, which induces high oscillations in the aerodynamic forces coefficients, when compared with results from URANS turbulence models which describe the average behavior of the fluid flow. It is interesting to note that the flow structures formed for a reduced frequency of $\kappa = 0.25$ are bigger and more chaotic than the structures formed in the previous simulation ($\kappa = 0.5$). As consequence the oscillations present on the aerodynamic coefficients are bigger, as can be observed in Fig. (4). Therefore, considering the turbulence modeling employed (Smagorinsky), a better procedure for this reduced frequency would be to simulate more pitching cycles and then apply a time average over the data, in order to obtain the mean behavior.

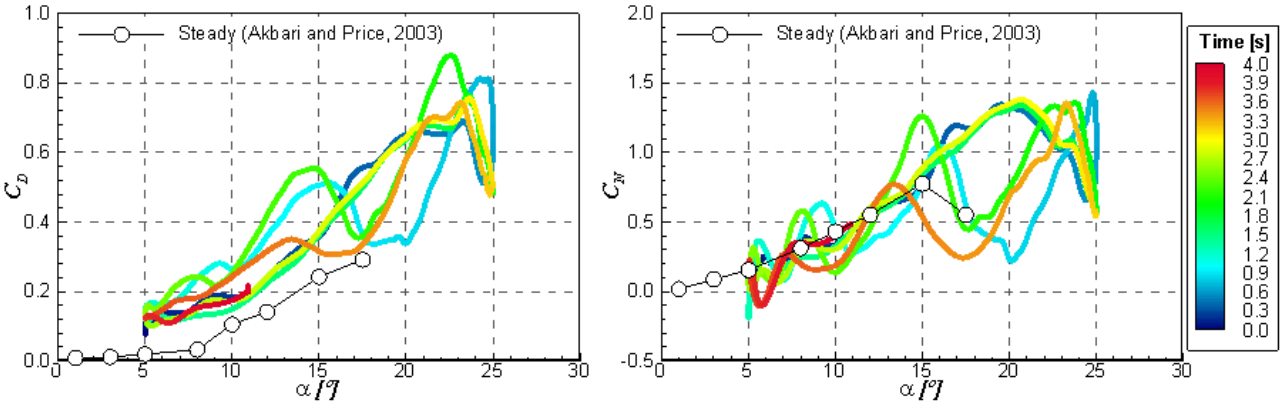

(a) (b)

Figure 4. The (a) drag and (b) normal force coefficients versus angle of attack over three oscillation cycles (4 s) for the airfoil at $\bar{\alpha} = 15^o$, $\Delta\alpha = 10^o$ and $\kappa = 0.25$

In the Fig. (5) a comparison between first oscillation cycle presented in Fig. (4) with the numerical simulations of Akbari and Prince (2003) is presented. The authors had used a re-meshing procedure to perform the pitching airfoil movement. The behavior of the normal force coefficient calculated in the present work with IB/VPM methodology is quite similar. Nevertheless, there are considerable differences between results that must be remarked. The dynamic stall during the upstroke was not observed in the classical method. The fluctuations in the normal coefficient are verified only in downstroke, presenting similar behavior with the results obtained using IB/VPM method but with smaller amplitudes. Another significant difference is the drag force coefficient that is clearly overestimated with relation the simulations results presented by Akbari and Prince (2003). However, any experimental reference for this Reynolds number was found to compare the differences between the two methodologies.

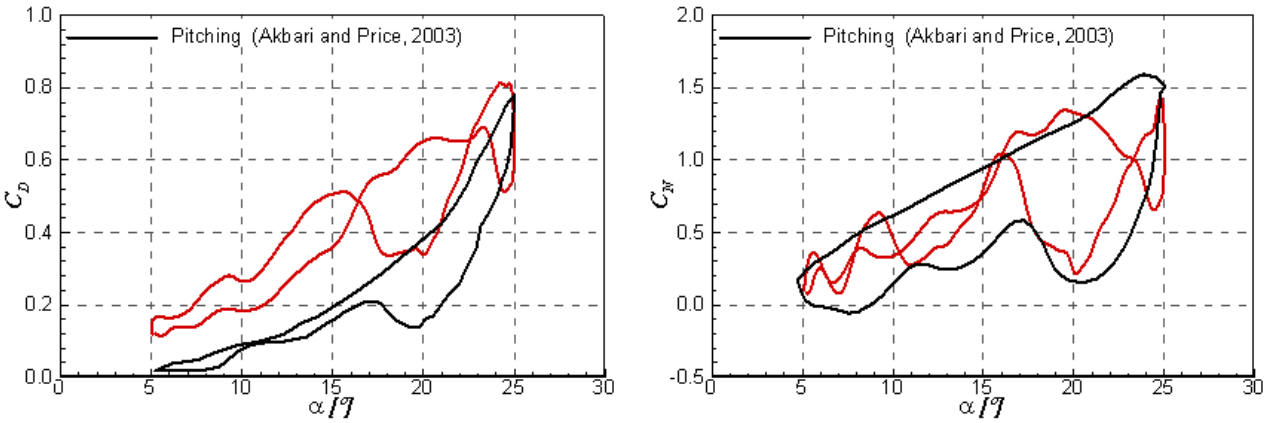

(a) (b)

Figure 5. The (a) drag and (b) normal force coefficients versus angle of attack, first oscillation cycle ($\kappa = 0.25$).

The vorticity fields for the first cycle of oscillations at reduced frequency of $\kappa = 0.25$ are presented in Fig. (6). Observing Fig. (6e) it is easy to see that the flow remains attached to the airfoil surface. At $\alpha = 19.2^o$ (Fig. 6f) the flow detaches from the airfoil, one leading-edge vortex is shedded and initiates the growth of separation bubble. When the airfoil reaches $\alpha = 22.4^o$ (Fig. 6g) the flow over the upper surface of the airfoil is completely separated, the second leading-edge vortex is fully formed and is shedded from the airfoil at about the mid-chord position. During the downstroke other high complex structures are formed from the upper surface of the

airfoil due the interaction between leading edge and trailing edge vortices (Fig. 6i-l). These structures prevent the flow reattachment. At the end of the cycle these structures are being advected downstream but the flow is still detached and small vortices are shedding (Kelvin-Helmholtz instabilities) from the leading edge (Fig. 6m-o).

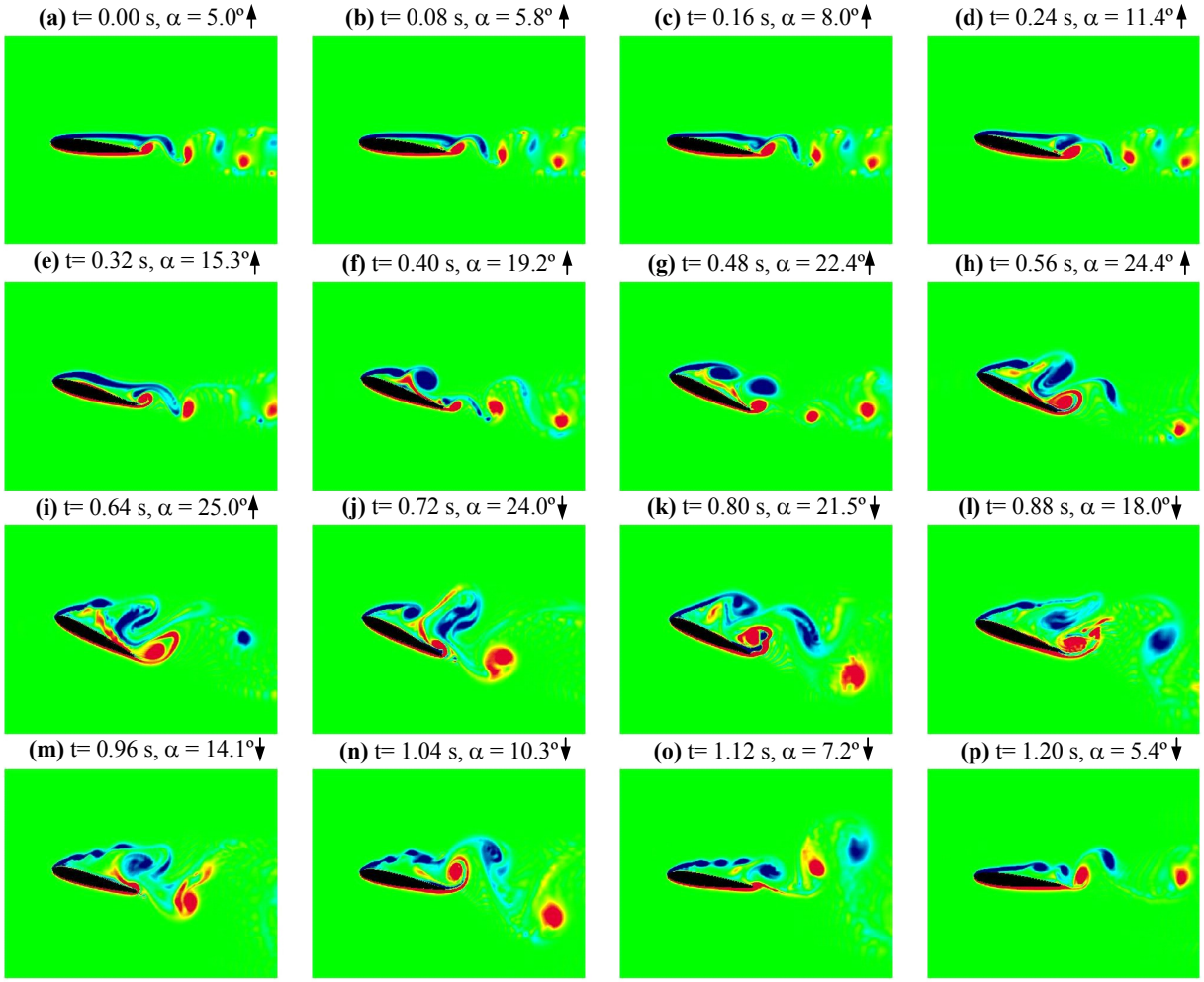

Figure 6. Vorticity field visualization at several angles of attack for a pitching NACA 0012 airfoil, at $\bar{\alpha} = 15^o$, $\Delta\alpha = 10^o$ and $\kappa = 0.25$

Comparing the two simulated cases we can observe some differences in the flow field between the first case, $\kappa = 0.5$, and the second case, $\kappa = 0.25$. In the first case the flow remains attached to airfoil during the most part of the upstroke (Fig. 3b–g), the leading-edge vortex is formed and released entirely during the downstroke, and only one trailing-edge vortex is shedded per cycle of oscillation. In both simulated cases it is interesting to note that the flow field remains "quiet" during the most part of the upstroke and much of the separation and vortex shedding activity occurs in the downstroke. This behavior is due to the influence of the airfoil movement that reduces the adverse pressure gradient in the upstroke cycle and increases it in the downstroke cycle.

6. Conclusions

In this work the IB/VPM was used to simulate pitching oscillations of a NACA 0012 airfoil, preliminary results are presented showing good coherence with the expected physical phenomena. It was performed two numerical simulations at two reduced frequencies 0.5 and 0.25, in order to evaluate the effect of the reduced frequency on the fluid flow. It was observed that increasing the reduced frequency of the pitching motion the flow separation was delayed to higher incidences compared to the static stall case. Separation was observed to start from the leading-edge, followed by the formation and advection of vortices along the surface of the airfoil, trailing-edge vortices were also observed to form and shed from the airfoil. Large amplitude oscillations were observed in the force coefficients for the simulation in the reduced frequency 0.25. This behavior was attributed to the Smagorinsky/LES turbulence model used. It is necessary more time of simulation to establish a trustworthy statistical data set. Significant differences between results of re-meshing method had been found and need to be better investigated.

7. Acknowledgements

The authors acknowledge CNPq and Fapemig for the financial support and the School of Mechanical Engineering of the Federal University of Uberlândia for the technical support.

8. References

Akbari, M. H. and Price, S. J. (2003). Simulation of dynamic stall for a NACA 0012 airfoil using a vortex method. Journal of Fluids and Structures, 17, 855–874.

Chorin, A. (1968). Numerical solution of the Navier-Stokes equations. Math. Comp. 22, 745–762.

Germano, M. (1986). A proposal for a redefinition of the turbulent stresses in filtered navier-stokes equations. Phys. Fluids 29(7), 2323–2324.

Lima e Silva, A. L. F., Silveira-Neto, A. and Damasceno, J. J. R. (2003). Numerical simulation of two dimensional flows over a circular cylinder using the immersed boundary method. Journal of Computational Physics 189, 351–370.

Peskin, C. S. (1977). Numerical analysis of blood flow in the heart. Journal of Computational Physics 25, 220–252.

Schneider, G. E. and Zedan, M. (1981). A modified strongly implicit procedure for the numerical solution of field problems. Numerical Heat Transfer 4, 1–19.

Silveira-Neto, A. (2003). Introdução Turbulência dos Fluidos, Apostila do Curso de Pós-Graduação em Eng. Mecânica. LTCM/FEMEC/UFU.

Smagorinsky, J. (1963). General circulation experiments with primitive equations. Monthly Weather Review 91, 99– 164.

9. Responsibility notice

The authors are the only responsible for the printed material included in this paper.